Reproduction

Reproduction (2024) **168** e240069
https://doi.org/10.1530/REP-24-0069

Received 1 March 2024
Accepted 24 June 2024
Available online 24 June 2024
Version of Record published 13 July 2024

RESEARCH

Dual role of valosin-containing protein (VCP/p97) in mouse sperm during capacitation

Martina Jabloñski[1], Florenza A La Spina[1], Liza J Schiavi-Ehrenhaus[1], Clara I Marín-Briggiler[1], Matias D Gomez-Elias[2], Dario Krapf[3], Pablo E Visconti[3], Diego Krapf[4], Guillermina M Luque[1] and Mariano G Buffone[1]

[1]Instituto de Biología y Medicina Experimental (IBYME), Consejo Nacional de Investigaciones Científicas y Técnicas (CONICET), Buenos Aires, Argentina
[2]Instituto de Biología Molecular y Celular de Rosario, CONICET-UNR, Rosario, Argentina
[3]Department of Veterinary and Animal Science, Paige Labs, University of Massachusetts, Amherst, Massachusetts, USA
[4]Department of Electrical and Computer Engineering and School of Biomedical Engineering, Colorado State University, Fort Collins, Colorado, USA

Correspondence should be addressed to M G Buffone; Email: mgbuffone@ibyme.conicet.gov.ar

Abstract

Valosin-containing protein (VCP; aka p97), a member of the AAA (ATPases Associated with various cellular Activities) family, has been associated with a wide range of cellular functions. While previous evidence has shown its presence in mammalian sperm, our study unveils its function in mouse sperm. Notably, we found that mouse VCP does not undergo tyrosine phosphorylation during capacitation and exhibits distinct localization patterns. In the sperm head, it resides within the equatorial segment and, following acrosomal exocytosis, it is released and cleaved. In the flagellum, VCP is observed in the principal and midpiece. Furthermore, our research highlights a unique role for VCP in the cAMP/PKA pathway during capacitation. Pharmacological inhibition of sperm VCP led to reduced intracellular cAMP levels that resulted in decreased phosphorylation in PKA substrates and tyrosine residues and diminished fertilization competence. Our results show that in mouse sperm, VCP plays a pivotal role in regulating cAMP production, probably by the modulation of soluble adenylyl cyclase activity.

Introduction

Following ejaculation, sperm are not immediately able to fertilize an egg. To achieve this task, they require to undergo several maturational steps in the female reproductive tract, collectively called sperm capacitation (Austin 1951, Chang 1951). Sperm capacitation involves complex signaling pathways that prepare sperm to develop hyperactivated motility and to undergo acrosomal exocytosis (aka acrosome reaction, AR) (Gervasi & Visconti 2016, Stival *et al.* 2016). Because sperm cells are transcriptionally and translationally silent, their regulatory signaling pathways largely depend on changes in intracellular ion concentrations, synthesis and degradation of second messengers, and protein post-translational modifications. The proteins that display either a change in localization or post-translational modification during capacitation are of particular interest because of their potential role in fertilization. Although the capacitation-induced molecular events have been intensively scrutinized in recent decades, many proteins modified during this process remain poorly understood.

Valosin-containing protein (VCP, aka p97) has been reported to undergo tyrosine phosphorylation and relocalization during capacitation in human sperm (Ficarro *et al.* 2003). VCP is a member of the AAA (ATPases Associated with various cellular Activities) family (Zhang *et al.* 2000) that has been implicated in a wide variety of cellular functions. It was initially recognized as one of the endoplasmic reticulum (ER)-associated proteins and has been shown to play critical roles in regulating ER formation and morphology by

Published by Bioscientifica Ltd.
https://rep.bioscientifica.com

Reproduction (2024) **168** e240069
https://doi.org/10.1530/REP-24-0069

participating in the ubiquitin–proteasome system (UPS) and other intracellular signaling pathways (Shih & Hsueh 2018). VCP has also been implicated in several fusion events in both yeast and mammalian cells (Kondo *et al.* 1997). Together with N-ethylmaleimide-sensitive factor (NSF) and syntaxin 5, VCP regulates the fusion of Golgi membranes (Rabouille *et al.* 1995). Even though VCP and NSF are highly homologous, they appear to participate in different fusion events, likely due to the participation of specific cofactors (Urbé *et al.* 1998). It was also reported that VCP has a role as a chaperone and aids in the assembly, disassembly, and functional operation of protein complexes (White & Lauring 2007). During T-cell activation, VCP undergoes tyrosine phosphorylation, which does not alter its ATPase activity (Egerton & Samelson 1994) but regulates its subcellular localization (Madeo *et al.* 1998). Moreover, tyrosine phosphorylation of VCP is required for membrane fusion processes such as transitional ER assembly *in vitro* (Hirling *et al.* 1996).

In human sperm, during the capacitation process, along with its phosphorylation on tyrosine residues, VCP changed its localization pattern. In noncapacitated (NC) human sperm, VCP localizes to the neck and tail regions. However, upon capacitation, fluorescent staining shows the appearance of VCP in the anterior head. VCP has also been proposed as a substrate of cAMP-activated boar sperm tyrosine kinase (Geussova *et al.* 2002), and it has been shown to participate in the autophagy and UPS of mitophagy after mammalian fertilization (Song *et al.* 2016).

In this article, we study the localization and function of VCP in mouse sperm. We show that VCP has a dual role in this species. First, VCP localizes in the equatorial segment (ES) of the sperm head and is cleaved and released after the AR. Second, contrary to what was observed for human, in mouse sperm, VCP does not undergo tyrosine phosphorylation on tyrosine residues during capacitation. Additionally, we found that VCP localizes to the flagellum and is involved in signaling events regulating the cAMP/PKA pathway, whose activation is required for capacitation.

Materials and methods

Reagents

Bovine serum albumin (BSA, A7906), α-β-tubulin (T4026), protease inhibitor cocktail (P8340), and progesterone (P8783) were purchased from Sigma-Aldrich, unless stated otherwise. Chemicals were obtained from the following sources: α-phosphotyrosine (α-pY) clone 4G10 from Millipore; horseradish peroxidase-conjugated (HRP) α-mouse IgG and HRP α-rabbit IgG from Vector Laboratories; FITC-conjugated goat α-mouse IgG (Thermo Scientific); NMS-873, ML-240 and DBeq from Cayman Chemicals (Ann Arbor, MI, USA); propidium iodide (PI) from Santa Cruz Biotechnology (USA) and α-VCP 612182 from BD Biosciences (USA). α-β-tubulin E7 was obtained from Developmental Studies Hybridoma Bank (DBHS, University of Iowa, USA). NMS-873, ML-240, DBeq, and progesterone were dissolved in DMSO; PI was dissolved in hexa-distilled water.

Animals

Hybrid F1 (C57BL/6 male × BALB/c female) mature (8–12-week-old) mice, as well as mature transgenic (BDF1-Tg (CAG-mtDsRed2, Acr3-EGFP) RBGS0020sb) male mice who have sperm with acrosomal vesicles expressing green EGFP fluorescence and mitochondria expressing red DsRed2 fluorescence (Hasuwa *et al.* 2010), were used. Animals were maintained at 23ºC with a 12 h light–12 h darkness cycle. Animal experimental procedures were reviewed and approved by the Ethical Committee of IBYME (CE/003-1/2011). Experiments were performed in strict accordance with the Guide for Care and Use of Laboratory Animals approved by the National Institutes of Health (NIH).

Sperm capacitation

The non-capacitating medium used in this study was a modified TYH medium, containing 119.3 mM NaCl, 4.7 mM KCl, 1.71 mM $CaCl_2{\cdot}2H_2O$, 1.2 mM KH_2PO_4, 1.2 mM $MgSO_4{\cdot}7H_2O$, 0.51 mM sodium pyruvate, 5.56 mM glucose, 20 mM 4-(2-hydroxyethyl)piperazine-1-ethanesulfonic acid (HEPES), and 10 µg/mL gentamicin (NC medium). This medium, which does not support capacitation, was prepared without BSA and $NaHCO_3$. Animals were euthanized and cauda epididymal mouse sperm were collected and placed in the NC medium. After 15 min of incubation at 37°C, epididymis were removed, and sperm were resuspended to a final maximum concentration of 10^7 cells/mL in the appropriate medium depending on the experiment performed. For capacitation, a medium containing 5 mg/mL of BSA and 15 mM of $NaHCO_3$ was used, and sperm were incubated at 37°C (CAP medium) for 90 min. In the cases where medium without added Ca^{2+} salts were required, 1.71 mM $CaCl_2{\cdot}2H_2O$ was omitted (nominal zero-Ca^{2+} medium, indicated by Ca^{2+} = 0). When chelation of the extracellular Ca^{2+} was needed, 1 mM EGTA was added at nominal zero-Ca^{2+} medium (indicated by Ca^{2+} = 0 + EGTA). In all cases, pH was adjusted to 7.4 with NaOH. To test the effect of inhibitors on capacitation, sperm were pre-incubated with inhibitors in the NC medium for 10 min prior to the beginning of the capacitating period.

Immunoblotting

After incubation in the appropriate medium, sperm were washed by centrifugation (5 min at 400 ***g***), resuspended in sample buffer without reducing agents

Reproduction (2024) **168** e240069
https://doi.org/10.1530/REP-24-0069

(62.5 mM Tris–HCl pH 6.8, 2% SDS, 10% glycerol), and boiled for 5 min. After centrifugation for 5 min at 13,000 ***g***, 5% β-mercaptoethanol and 0.0005% bromophenol blue were added to the supernatants then boiled again for 5 min. Protein extracts equivalent to 2–4 × 10^6 sperm per lane were separated by SDS-PAGE in gels containing 10% polyacrylamide and transferred onto nitrocellulose membranes. Blots were blocked in 5% nonfat dry milk in PBS containing 0.1% Tween 20 (T-PBS) for 1 h at room temperature. An overnight incubation at 4ºC with the first antibody was required. Antibodies were diluted in 2% nonfat dry milk in T-PBS as follows: α-VCP (1:1000), α-pPKAs (1:3000), α-pY (1:3000), and α-β-tubulin (1:3000). The corresponding secondary antibodies were incubated for 45 min at room temperature, diluted in 2% nonfat dry milk in T-PBS as follows: 1:1000 for HRP α-rabbit and 1:4000 for HRP α-mouse. In all the cases, the reactive bands were detected by enhanced chemiluminescence (GE Healthcare, USA). When necessary, membranes were stripped for 10 min in 2% SDS, 0.67% β-mercaptoethanol, and 62.5 mM Tris pH 6.8. In all experiments, molecular masses were expressed in kilodaltons (kDa). As a loading control, α-β-tubulin was used. For band quantification, rectangular boxes were drawn around bands on scanned digital images of ECL contact photographs of Western blots. Adjusted optical densities for each lane were obtained using ImageJ (NIH).

Immunoprecipitation

Immunoprecipitation was performed as previously described with minor modifications (Stival *et al.* 2015). After sperm incubation in the appropriate conditions, samples were centrifuged at 1700 ***g*** for 1 min. The resulting pellet was resuspended in RIPA buffer (10 mM Tris-HCl pH 7.2, 50 mM NaCl, 0.1% SDS, 1% Triton X-100, 1 mM EDTA, 1 mM sodium orthovanadate, and protease inhibitors), incubated on ice for 30 min, and centrifuged at 4°C for 5 min at 2500 ***g***. Supernatants were incubated sequentially (after stripping) with α-VCP or α-pY antibodies (1:200 of antibody for 10^7 cells in a final volume of 500 µL) for 2 h at room temperature with constant rocking. After adding 20 µL protein G-sepharose (GE Healthcare), the reactions were further rocked for 1 h at 4°C. The immune complex was recovered by centrifugation, washed four times in RIPA buffer, and subjected to SDS/PAGE and Western blot. To avoid immunoreactive signals from denatured IgGs used for immunoprecipitation, a monoclonal secondary-HRP mouse α-native rabbit IgG was used (clone RabT-50, Sigma). Input refers to the total protein used for IP.

Immunofluorescence and super-resolution microscopy

To perform immunofluorescence on mouse sperm, we used a previously described method (Romarowski *et al.* 2015). Briefly, mouse sperm obtained from cauda epididymis and capacitated during different times were washed twice by centrifugation for 5 min at 400 ***g***, resuspended in PBS, and placed onto cover slides. Sperm were air-dried and then treated with PBS containing 4% formaldehyde for 15 min at room temperature. After washing twice for 5 min in T-PBS, sperm were permeabilized with 0.5% Triton X-100 in PBS for 5 min. The slides were then washed twice for 5 min and incubated in T-PBS containing 10% normal goat serum (blocking buffer) for 1 h at room temperature, then with primary antibody (1:100; purified mouse α-VCP) diluted in T-PBS containing 1% normal goat serum for an overnight period at 4°C. Following a washing step (three times, 5 min in T-PBS), slides were incubated with FITC-conjugated goat α-mouse IgG diluted 1:200 in T-PBS containing 1% normal goat serum for 1 h at room temperature, washed again for three times, and mounted using Vectashield (Vector Labs, USA). Non-specific staining was determined by incubating the sperm with rabbit IgG. Samples were examined using either a laser scanning confocal microscope (Nikon C1 Eclipse 800) equipped with a 60× objective (NA 1.4) or a NanoImager S microscope (Oxford Nanoimaging Ltd), equipped with a 100× oil-immersion objective (NA 1.4, Olympus) and a sCMOS camera (Hamamatsu ORCA-Flash4.0 V3 Digital CMOS camera).

CatSper opening through determination of membrane potential by flow cytometry

Sperm E_m changes were assessed using $DiSC_3(5)$ as previously described (Puga Molina *et al.* 2018, Luque *et al.* 2023). Briefly, after a 20-min incubation with VCP inhibitors (20 µM NMS-873, 1 µM ML-240, or 5 µM DBeq), CatSper inhibitor (as a negative control, 20 µM HC-056456) or vehicle (DMSO), 50 nM $DiSC_3(5)$ was added. In these experiments, $DiSC_3(5)$ was not washed. To monitor viability, 3 µM of PI was added before measurement. Data were recorded as individual cellular events using a BD FACSCanto II™ cytometer (Biosciences; Becton, Dickinson and Company). Basal E_m was obtained after 30 s of continuous recording, followed by chelation of Ca^{2+} with 3.5 mM of EGTA. Then, acquisition continued for an additional 150 s. Positive cells for $DiSC_3(5)$ were collected using the filter for allophycocyanin (APC; 660/20), and for PI using the filter for peridinin chlorophyll protein complex (PerCP; 670LP). Compensation was done. Data were analyzed using FlowJo software (V10.0.7).

Determination of intracellular cAMP levels

After the incubation of sperm in the appropriate conditions for 12 min, reactions were stopped by centrifugation at 2000 ***g*** for 3 min at room temperature. Cells were resuspended with 200 µL of 0.1 M HCl and lysed for 10 min at room temperature. Sperm lysates were centrifuged at 2000 ***g*** for 3 min and the cAMP in the supernatant was acetylated and quantified using the Direct cAMP ELISA Kit (Enzo, Farmingdale, NY,

Reproduction (2024) **168** e240069
https://doi.org/10.1530/REP-24-0069

USA; Catalog # ADI-901-066A) according to the manufacturer's instructions. This ELISA-based assay has an increased sensitivity of 0.006 pmol/mL cAMP in the acetylated assay format. A standard curve was run for each assay and the unknown cAMP concentrations were obtained by interpolation as recommended by the manufacturer.

Computer-assisted sperm analysis

After incubation in the appropriate conditions, sperm suspensions were loaded on a 100 µm depth chamber slide (Leja Slide, Spectrum Technologies) and placed on a microscope (Nikon Eclipse E200) stage at 37°C coupled to a Basler acA780-75gc camera. Sperm movements were examined using a CASA system (Sperm Class Analyzer: SCA evolution, Microptic, Spain). Parameters used were as follows: 30 frames acquired, frame rate of 60 Hz, and cell size of 30–170 μm^2. At least 20 microscopy fields corresponding to a minimum of 200 sperm were analyzed in each experiment. The following parameters were measured: mean path velocity (VAP), curvilinear velocity (VCL), straight line velocity (VSL), linearity (LIN), amplitude of lateral head displacement (ALH), and straightness (STR).

Acrosomal exocytosis

AR was assessed as previously described (Hirohashi *et al.* 2015). Briefly, mt-DsRed2 Acr-EGFP mouse sperm were resuspended to a final maximum concentration of 10^7 cells/mL on NC medium. A 10-min preincubation in NC medium containing inhibitors was conducted when required. After that, sperm were incubated under CAP conditions for 60 min in the presence or absence of inhibitors. At 60 min of incubation, progesterone (30 µM) or A23187 (10 µM) was added for 30 min to induce the AR. Before collecting data, 2 µg/mL propidium iodide was added to monitor viability. Data were recorded as individual cellular events using a BD FACSCanto II TM cytometer (Biosciences; Becton, Dickinson and Company). Side-scatter area and forward-scatter area data were collected from 20,000 events per sample to define sperm population. In all cases, doublet exclusion was performed by analyzing the two-dimensional dot plot forward-scatter area vs forward-scatter height. Positive cells for EGFP were collected using the filter for FITC (530/30) and for propidium iodide, using the filter for peridinin chlorophyll protein complex (670LP). The two indicators had minimal emission overlap, but compensation was still done. Data were analyzed using FlowJo software (V10.0.7).

In vitro fertilization

Eight-to-12-week-old F1 female mice were superovulated using equine chorionic gonadotropin (5 IU, PMSG; Syntex), followed 48 h later by human chorionic gonadotropin (5 IU, hCG; OVUSYN, Syntex) intraperitoneal injection. Cumulus–oocyte complexes (COCs) were collected from oviducts 13–14 h after hCG administration, placed in TYH IVF medium (containing 25 mM $NaHCO_3$ and 4 mg/mL of BSA, with no HEPES addition). Sperm were capacitated *in vitro* at a final concentration of 5×10^5 sperm/mL in the presence or absence of 20 µM NMS-873. Once capacitated, sperm were washed by centrifugation for 5 min at 400 ***g***, resuspended in fresh TYH CAP medium, and used to inseminate COCs. After coincubation for 4 h at 37°C with 5% CO_2, eggs were washed three times and placed in drops containing TYH IVF at 37°C with 5% CO_2. Fertilization was assessed by the visualization of two-cell embryos 20 h later.

Statistical analysis

Data are expressed as mean ± S.E.M. of at least three experiments for all determinations. Statistical analyses were conducted using GraphPad Prism v4.0 (USA). The specific statistical analysis employed is indicated in the figure legends. A *P*-value of less than 0.05 ($P < 0.05$) was considered statistically significant.

Results

VCP localized to the equatorial segment and to the flagellum of mouse sperm

In mouse sperm, the α-VCP antibody recognized a single band for the expected size (97 kDa) by Western blot (Fig. 1A). Immunolocalization revealed remarkable differences compared to human sperm (Ficarro *et al.* 2003). VCP is localized in the ES of the mouse sperm head and in the sperm flagellum (Fig. 1B). Localization in the head was confirmed using transgenic Acr3-EGFP-sperm, with the strong VCP signal in the ES while EGFP was mostly restricted to the anterior acrosomal cap (Fig. 1C).

VCP is not tyrosine phosphorylated during mouse sperm capacitation

In contrast to what was reported in human sperm (Ficarro *et al.* 2003), mouse sperm VCP did not change its ES localization during capacitation (Fig. 2A). Because of the differences observed in the localization of VCP in mouse and human sperm, we investigated if VCP is tyrosine phosphorylated during capacitation. To that end, an α-VCP was used for immunoprecipitation of non-capacitated (NC) as well as of capacitated sperm protein extracts. Sperm of each population were extracted and immunoprecipitated using α-VCP and the immunoprecipitates were then probed with both α-pY and α-VCP by immunoblotting, as shown in Fig. 2B. Overall, this experiment confirmed that VCP was

Reproduction (2024) **168** e240069
https://doi.org/10.1530/REP-24-0069

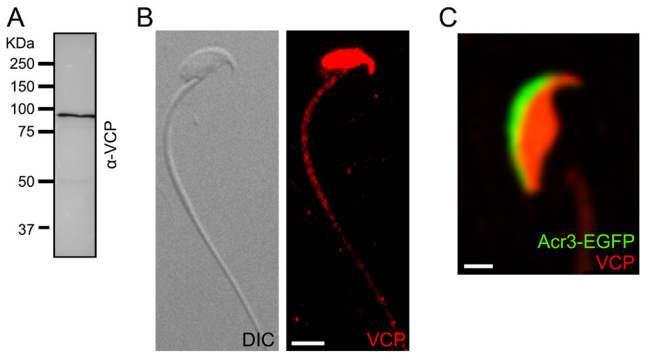

Figure 1

VCP is expressed in mouse sperm and localized in the equatorial segment and the flagellum. (A) Mouse sperm proteins were analyzed by 10% SDS-PAGE and immunoblotted using an antibody against VCP. The lane contained 5 × 10^6 sperm. (B) Immunofluorescence showing the localization of VCP in mouse sperm incubated under non-capacitating (NC) conditions. Scale bar = 5 µm. A representative image of at least three independent experiments is shown. (C) Immunofluorescence showing the localization of VCP in transgenic Acr3-EGFP mouse sperm. Scale bar = 2 µm.

effectively immunoprecipitated by the α-VCP antibody since a single band of the expected molecular size (97 kDa) was detected in both NC and capacitated (CAP) sperm extracts (Fig. 2B, left panel). However, these bands were not observed when the membrane was probed with an α-pY antibody (Fig. 2B, right panel) indicating that VCP does not undergo tyrosine phosphorylation during capacitation.

VCP is released and cleaved during the course of the acrosome reaction

Due to the localization of VCP in the ES of mouse sperm, we investigated its fate during either induced or spontaneous AR. To this end, transgenic Acr-EGFP exposed to agonists of AR (progesterone or the Ca^{2+} ionophore A23187) were fixed and stained with α-VCP. In Fig. 3A, a representative set of images corresponding to this experiment is shown. Most of the acrosome-intact sperm exhibited VCP in the ES. However, those that underwent AR lost the VCP signal in the ES (see quantification in Fig. 3B). Despite VCP being lost after AR, the signal in the flagellum remained unaltered, as shown in Fig. 3C.

Next, we investigated if this protein is released to the surrounding medium. After the incubation in CAP conditions, the suspension of sperm undergoing spontaneous or induced AR was centrifuged, and the supernatant was analyzed by immunoblotting using α-VCP. We observed the presence of a 58 kDa VCP fragment in the supernatant of sperm incubated under CAP conditions in those that underwent either induced or spontaneous AR, suggesting the release of this fragment (Fig. 3D). In contrast, the presence of the full-length 97 kDa form was not observed. A previously reported *in silico* analysis of the VCP sequence demonstrated the presence of two cleavage sites for trypsin-like proteases that produce VCP fragments of 58 and 87 kDa (Halawani *et al.* 2009), which match those observed in our experimental conditions (Fig. 3D). As a control, media recovered from sperm that swam out from the cauda epididymis in NC medium did not show the presence of VCP evidenced by the absence of the band corresponding to VCP. The 87-kDa form is barely observed in those sperm released from the cauda epididymis (see first lane) and could not be observed after exposure to CAP medium.

Inhibition of VCP led to reduced protein tyrosine phosphorylation

We further explored the role of VCP in the flagellum using different pharmacological inhibitors against

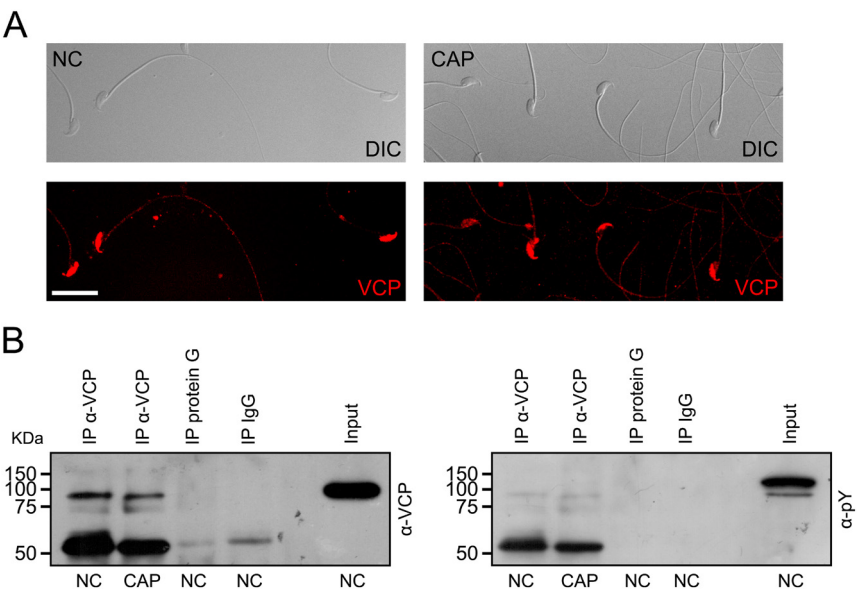

Figure 2

VCP is not phosphorylated in tyrosine residues during capacitation. (A) Immunofluorescence showing the localization of VCP in mouse sperm incubated under capacitating (CAP) or non-capacitating (NC) conditions. Representative images of at least three independent experiments are shown. Scale bar = 20 µm. (B) Sperm incubated in CAP and NC media were extracted with RIPA buffer and immunoprecipitated with α-VCP. Immunocomplexes were subjected to 10% SDS/PAGE, transferred to PVDF membranes and developed two times (after stripping) with either α-VCP (left panel) or α-pY (right panel). Input refers to the total protein used for IP.

Reproduction (2024) **168** e240069
https://doi.org/10.1530/REP-24-0069

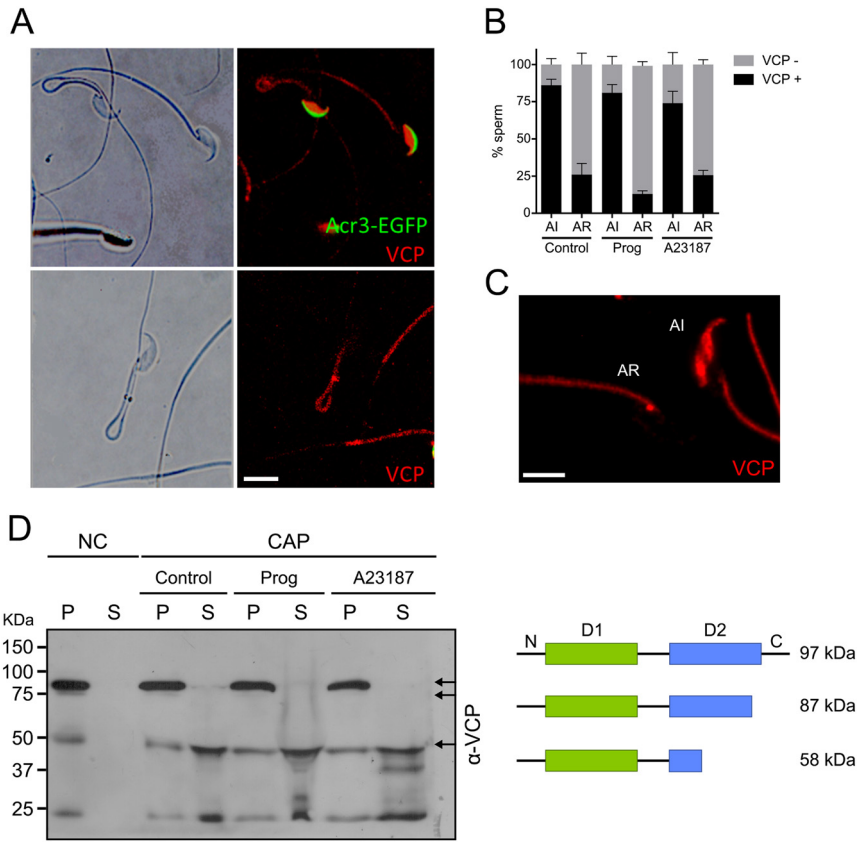

Figure 3

VCP is cleaved and released from the ES during AR. (A) Capacitated Acr3-EGFP sperm were incubated under CAP conditions followed by exposure to 30 µM progesterone to induce acrosome reaction. Then, sperm were fixed, attached to a slide and stained with α-VCP antibody followed by α-mouse TRITC. Slides were observed using a confocal microscope. Scale bar = 10 µm. (B) Percentage of sperm that display a positive or negative signal for VCP (VCP+, VCP−, respectively) in the equatorial segment in the acrosome-intact (AI) or acrosome-reacted (AR) population. Sperm were analyzed in different conditions: after the incubation under CAP conditions (control); after the incubation under CAP conditions and stimulated with either progesterone (Prog 30 µM) or A23187 (10 µM). Data from at least three independent experiments are shown with 100 cells analyzed. (C) Immunofluorescence showing the localization of VCP in AI and AR mouse sperm. Note how, although lost in the head, VCP remains in the flagellum after AR. Scale bar = 5 µm. (D) Left panel: Equal number of mouse sperm were incubated under NC and CAP conditions for up to 90 min. A subset of cells was then stimulated with progesterone (30 µM) or A23187 (10 µM). Then, the incubation mixture was separated into a pellet (P) and supernatant (S) and analyzed by 10% SDS-PAGE and immunoblotting with α-VCP. The α-VCP antibody detected molecular bands of ~97, ~87, and 58 kDa. The experiment was repeated at least three times. Right panel: Schematic representation of VCP in mouse sperm. The 97 kDa monomer is composed of two contiguous domains (domain 1 D1 and domain 2 D2) (Halawani *et al.* 2009).

this protein. These inhibitors possess different mechanisms of action. NMS-873 is a highly selective allosteric inhibitor that acts by binding to the interface of two adjacent domains within the active hexameric structure of VCP and leads to an interruption of its catalytic cycle by stabilizing the ADP-bound state (Bouwer *et al.* 2021). As for DBeq, it was identified as a selective, potent, reversible, and ATP-competitive VCP inhibitor that targets both D1 and D2-ATPase domains of VCP (Chou *et al.* 2011, Fang *et al.* 2015). In contrast, ML-240, derived from the scaffold of DBeq, only targets the D2-ATPase domain (Fang *et al.* 2015).

We used these inhibitors to investigate if VCP plays a role in regulating phosphorylation events that take place in the flagellum mediated by the cAMP/PKA pathways. As depicted in Fig. 4A and Supplementary Fig. 1 (see section on supplementary materials given at the end of this article), the incubation of sperm for 90 min under CAP conditions with increasing concentrations of the three inhibitors resulted in reduced tyrosine phosphorylation levels in a concentration-dependent manner. The maximum concentration tested for each VCP pharmacological inhibitor was chosen as 20 µM for NMS-873, 1 µM for ML-240, and 5 µM for DBeq.

To better understand the role of VCP in PKA activity, we subjected sperm to a challenge by chelating extracellular Ca^{2+}. In the complete absence of extracellular Ca^{2+}, as seen in conditions with EGTA, tyrosine phosphorylation levels experience a significant increase, but only if PKA is active (Navarrete *et al.* 2015). Consequently, in Fig. 4B and Supplementary Fig. 2, the presence of VCP inhibitors leads to a decrease in tyrosine phosphorylation when exposed to EGTA, providing further support for the notion that VCP operates upstream of PKA action.

Partial inhibition of CatSper channels by VCP inhibitors might lead to a decrease in tyrosine phosphorylation, akin to the conditions observed when sperm are incubated with low concentrations of Ca^{2+} (Navarrete *et al.* 2015). One way of evaluating CatSper activity indirectly is by measuring E_m changes after removing external free divalent cations by chelation with EGTA. This will cause CatSper to efficiently conduct

Reproduction (2024) **168** e240069
https://doi.org/10.1530/REP-24-0069

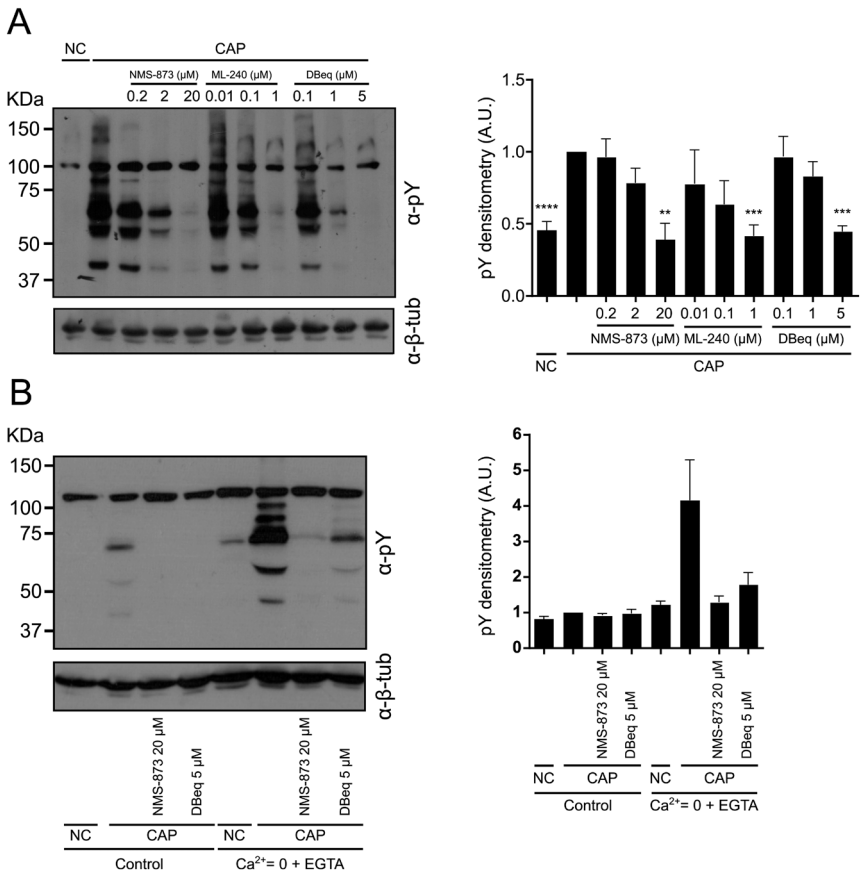

Figure 4

VCP inhibition abolished sperm protein tyrosine phosphorylation during capacitation. (A) Protein extracts were separated by 10% SDS-PAGE and immunoblotted with an antibody against pY. As a loading control, β-tubulin was used. Sperm were incubated for 90 min under NC or CAP conditions in the absence (DMSO) or presence of VCP inhibitors. Quantitative analysis was performed by measuring the optical density of all bands and relativized to β-tubulin. Data are presented mean ± S.E.M. of at least three independent experiments, where normalization to the control condition (CAP 90 min with DMSO) was used. ****$P < 0.0001$ represents statistical significance vs control (CAP 90 min with DMSO). Non-parametric Kruskal–Wallis test was performed in combination with Dunn's multiple comparisons test. (B) Protein extracts were separated by 10% SDS-PAGE and immunoblotted with an antibody against pY. As a loading control, β-tubulin was used. Sperm were incubated for 90 min under NC and CAP in the absence (DMSO) or presence of VCP inhibitors (20 μM NMS-873 and 5 μM DBeq). In addition, two different media were used: (a) complete TYH medium (control); (b) medium without added Ca^{2+} salts (nominal zero-Ca^{2+} medium, Ca^{2+}= 0) with EGTA 1 mM (Ca^{2+}= 0 + EGTA). Quantitative analysis was performed by measuring the optical density of all bands and relativized to β-tubulin. Data are presented as mean ± S.E.M. of at least three independent experiments, where normalization to the control condition (CAP 90 min with DMSO) was used. Non-parametric Friedman test was performed in combination with Dunn's multiple comparisons test.

monovalent cations such as Na^+ when it is open. Since Na^+ is highly concentrated in the extracellular milieu, a sudden influx depolarizes the cell, and it can be measured with the cationic dye $DiSC_3(5)$ by flow cytometry. Our experiments depicted in Supplementary Fig. 4A demonstrate that VCP inhibitors do not impact CatSper function, evidenced by the lack of alteration in the depolarization of the E_m in response to EGTA (Luque *et al.* 2021, Luque *et al.* 2023), in contrast to the CatSper inhibitor HC-056456.

Diminished cAMP levels and PKA activation as a result of VCP inhibition

To investigate if VCP inhibition alters the capacitation-induced PKA activation, sperm were incubated under CAP conditions in the presence of the VCP inhibitor NMS-873, and PKA-dependent phosphorylation was evaluated. Incubation with NMS-873 led to a decrease in the phosphorylation of PKA substrates (Fig. 5A) suggesting that active VCP is essential for proper PKA activity. To verify that the action of VCP is upstream PKA activation, sperm were incubated under CAP conditions with NMS-873, followed by the addition of increasing concentrations of the membrane-permeable cAMP analog, 8-Br-cAMP. Under these conditions, the levels of PKA substrates and tyrosine phosphorylation were increased in a concentration-dependent manner reaching levels comparable to the control CAP condition (Fig. 5A). The same behavior of a decrease in PKA substrates phosphorylation is seen when Dbeq and ML-240 are used to inhibit VCP and, as observed with NMS-873, this inhibition is rescued by increasing concentrations of 8-Br-cAMP (Supplementary Fig. 4). These findings indicate that VCP regulates the signals essential for the occurrence of PKA activation, acting upstream PKA.

To further explore the role of VCP on PKA activation, intracellular cAMP levels were examined when sperm were exposed to both NC and CAP, while being treated with NMS-873. As illustrated in Fig. 5B, intracellular cAMP levels exhibited a rapid increase when sperm were incubated under CAP conditions. However, the presence of the VCP inhibitor NMS-873 entirely abolished this increase in intracellular cAMP, resulting in levels akin to those observed in NC

Reproduction (2024) **168** e240069
https://doi.org/10.1530/REP-24-0069

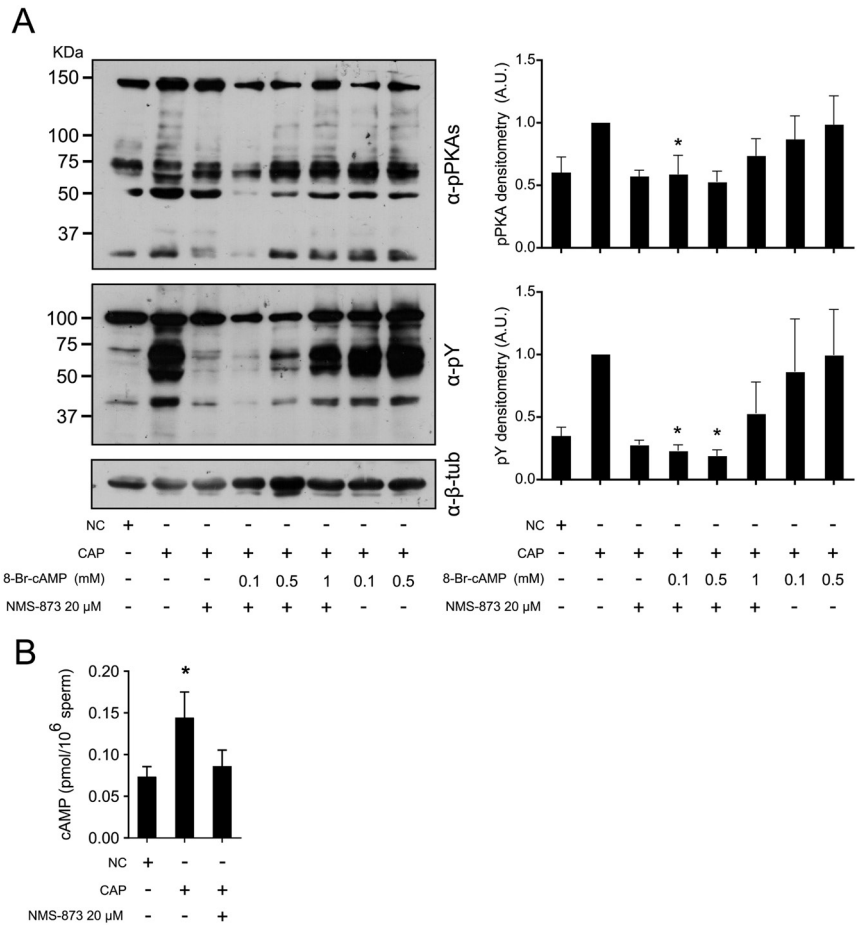

Figure 5

cAMP levels are reduced in the presence of VCP inhibitors. (A) Protein extracts were separated by 10% SDS-PAGE and immunoblotted with antibodies against substrates phosphorylated by PKA (pPKAs) and pY. As a loading control, β-tubulin was used. Sperm were incubated for 90 min under NC or CAP in the absence (DMSO) or presence of 20 μM NMS-873 together with increasing concentrations of 8-Br-cAMP (0.1, 0.5, and 1 mM). Quantitative analysis was performed by measuring the optical density of all bands and relativized to β-tubulin. Values represent the mean ± S.E.M. of at least three independent experiments, where normalization to the control condition (CAP 90 min with DMSO) was used. *P < 0.05 represents statistical significance vs control (CAP 90 min with DMSO). Non-parametric Friedman test was performed in combination with Dunn's multiple comparisons test. (B) Total intracellular cAMP content of sperm incubated for 90 min under NC or CAP conditions with or without 20 μM NMS-873. Values represent mean ± S.E.M. of four independent experiments. *P < 0.05 represents statistical significance vs control (CAP 90 min with DMSO). Non-parametric Friedman test was performed in combination with Dunn's multiple comparisons test.

conditions. Altogether, these results suggest that VCP activity is required for maintaining the capacitation-associated rise in intracellular cAMP levels.

VCP inhibition impairs the rate of acrosomal exocytosis and decreases the fertilization rate in IVF without affecting sperm motility

Sperm were subjected to incubation under capacitating conditions while exposed to increasing concentrations of the VCP inhibitor NMS-873. As illustrated in Supplementary Fig. 4C and Supplementary Table 1, there were no significant differences observed in sperm motility as assessed by computer-assisted sperm analysis (CASA).

AR was assessed by exposing sperm to increasing concentrations of NMS-873 when incubated under CAP conditions followed by the addition of either 30 μM progesterone or 10 μM A23187. As shown in Fig. 6A, a progressive inhibition of the progesterone-induced AR was observed, and it became statistically significant at the concentration of 2 μM. In contrast, no inhibition was noted when sperm were challenged with calcium ionophore.

Finally, IVF experiments were conducted in the presence of 20 μM NMS-873, and the results were compared to those of the control group (vehicle). As shown in Fig. 6B, sperm that had been pre-incubated with the VCP inhibitor exhibited lower fertilization rates when compared to the control sperm.

Discussion

In the present work, we analyzed the role of VCP in mouse sperm. First, we found that the localization of this protein in different compartments of the mature sperm. The first evidence related to this protein in mammalian sperm shows that it is localized in the neck and tail of human sperm, and that during capacitation, VCP is relocalized to the anterior acrosome (Ficarro *et al.* 2003). In mouse sperm, we observed a different localization; in this species VCP localized to the ES and the flagellum, and this pattern is not altered during capacitation. The area corresponding to the equatorial segment of the sperm head is of great importance for mammalian fertilization since fusion between the sperm plasma membrane and the egg's oolemma takes place in this region. As such, key proteins for sperm–egg fusion such as IZUMO1 are relocalized to

Reproduction (2024) **168** e240069
https://doi.org/10.1530/REP-24-0069

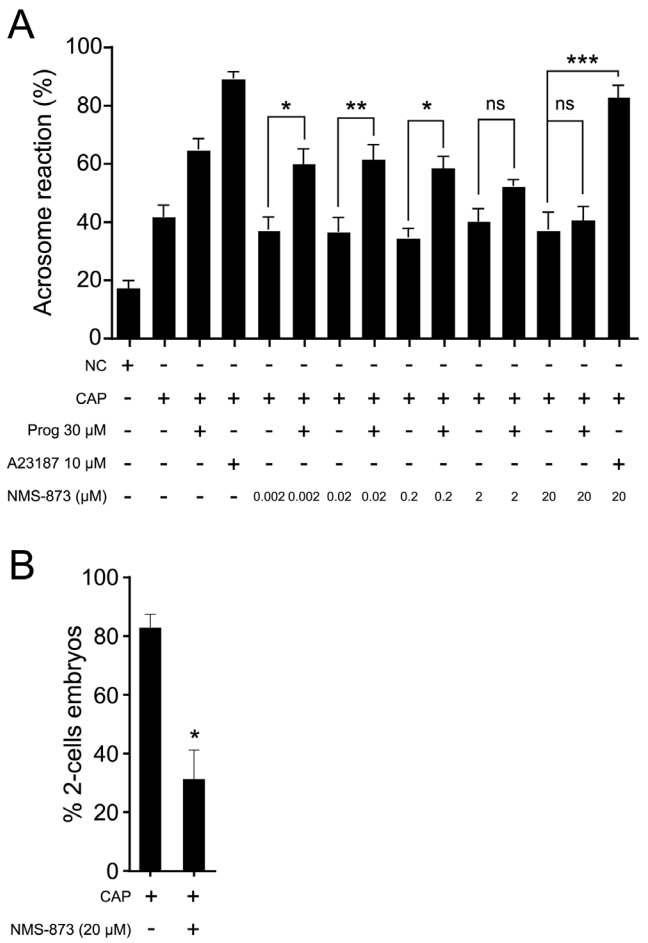

Figure 6

Effect of VCP inhibitor NMS-873 on acrosome reaction and IVF. (A) Acrosome reaction was assessed by flow cytometry analysis of Acr-EGFP sperm. Mouse sperm were incubated for 90 min under CAP conditions in the absence (DMSO) or presence of increasing concentrations of NMS-873. At 60 min of incubation, progesterone or A23187 were added to stimulate acrosome reaction. The percentage of live sperm that undergo acrosome reaction is shown. Results are expressed as the mean ± S.E.M. of at least six independent experiments. **P* < .05 represent statistical significance vs control (Pg). One-way ANOVA was performed in combination with Dunnett's multiple comparisons test. (B) IVF was performed using sperm that were preincubated with DMSO (control) or 20 µM NMS-873. Data represents mean ± S.E.M. of at least four independent experiments. **P* < .05 and ***P* < .01 represent statistical significance vs conditions without progesterone. Paired *t*-test was performed.

this region after AR (Miranda *et al.* 2009, Satouh *et al.* 2012). Other proteins that have been reported to migrate to the ES in mouse sperm are CD81 (Jankovicova *et al.* 2016), CAPZA3 (Sosnik *et al.* 2010), CRISP1/2 (Busso *et al.* 2007), α-L-Fucosidase, SLLP1 (Mandal *et al.* 2003, Herrero *et al.* 2005), fertilin β (Hunnicutt *et al.* 1997), and equatorin (Toshimori *et al.* 1992). However, to the best of our knowledge, with the exception of TMEM225 (Matsuura & Yogo 2015) and Capza3 (Sosnik *et al.* 2010), all the proteins that are a constitutive part of the ES or that are relocalized to this region are not lost after the AR. In fact, it is possible that the major reorganization that takes place in the plasma membrane during capacitation promotes the breakdown of the diffusion barriers between domains, allowing protein migration to the ES (Flesch *et al.* 2000, Gadella 2008). Proteins located in the acrosome, on the other hand, could either migrate to the ES via the 'hairpin' structure formed by the acrosomal and plasma membranes in the equatorial sheath after the AR (Leung *et al.* 2021). Here, we show that VCP is lost after the AR and further experiments are needed to clarify in detail the subcellular localization and understand the mechanisms by which some proteins are lost while others remain attached to this area.

As previously mentioned, in humans, VCP is phosphorylated in tyrosine residues during capacitation (Ficarro *et al.* 2003). In this manuscript, it was speculated that this phosphorylation may be linked to the migration of VCP to the acrosomal cap. This hypothesis is based on results obtained in other systems where VCP undergoes tyrosine phosphorylation during T-cell activation. In these cells, although phosphorylation did not alter its ATPase activity, it regulates the subcellular localization of this protein. In the mouse, VCP is not phosphorylated in tyrosine residues during capacitation, which may be consistent with the lack of change in localization during capacitation.

Another finding that emerged from our experiments is that VCP is cleaved after it is released to the surrounding medium. A previously published *in silico* analysis suggests that the observed fragments are compatible with target sequences for trypsin or trypsin-like proteases (Halawani *et al.* 2009). One of the sperm-specific trypsin-like proteases is acrosin. This enzyme is one of the many acrosomal proteases responsible for digesting specific acrosomal components such as ZP3R/sp56 (Buffone *et al.* 2008, *et al.* 2009).

Regarding the role of VCP in the sperm flagellum, where most of the tyrosine phosphorylated and PKA-induced phosphorylated substrates localized, experiments using inhibitors against VCP showed that PKA substrates and tyrosine phosphorylation are substantially reduced. In the complete absence of Ca^{2+} such as in CatSper KO sperm, in the presence of CatSper inhibitors or by adding EGTA, tyrosine phosphorylation levels increase dramatically. Our hypothesis is that VCP is positively helping the occurrence of tyrosine phosphorylation. To further support this hypothesis, extracellular Ca^{2+} was removed by the addition of EGTA. This treatment greatly increases the levels of tyrosine phosphorylation when PKA is active (Navarrete *et al.* 2015). However, in conditions where VCP was inhibited, the EGTA-induced increase was almost completely obliterated.

Capacitation and, therefore, the preparation for the AR is also regulated by cAMP-dependent pathways

(Visconti *et al.* 1995). Thus, the altered induction of the AR is consistent with the low levels of cAMP assessed in the presence of VCP inhibitors. Similarly, the inhibition of PKA-dependent phosphorylation explains the block on tyrosine phosphorylation, a process mediated by FERT (Alvau *et al.* 2016). Also, the block of capacitation-induced cAMP-dependent pathway is consistent with the significant reduction of IVF rates. We did not observe a complete block of fertilization in these conditions; this result is probably due to the dilution of the inhibitor concentration in the fertilization droplet.

Our results are consistent with VCP involvement in the regulation of cAMP-dependent pathways. In addition, VCP cleavage and loss from the ES after the AR suggest alternative regulation of this protein during exocytosis. Future experiments will be necessary to unravel the molecular mechanisms underlying VCP's involvement in these two functions.

Supplementary materials
This is linked to the online version of the paper at https://doi.org/10.1530/REP-24-0069.

Declaration of Interest
The authors declare that there is no conflict of interest that could be perceived as prejudicing the impartiality of the research reported. MGB is an Associate Editor of *Reproduction*. MGB was not involved in the review or editorial process for this paper, on which he is listed as an author.

Funding
This work was supported by the National Institutes of Health (NIH R01HD106968 to MGB and DK; NIH-HD088571 to PEV and HD38082 to PEV), *Agencia Nacional de Promoción Científica y Tecnológica* (PICT 2020-00098, 2021-00031) *Consejo Nacional de Investigaciones Científicas y Técnicas* (PIBAA 2022-100368 to GML), and Chan Zuckerberg Initiative (CZI 2021–240504).

Author contribution statement
MJ, FALS, JSE performed experiments and analyzed data; MGE and CLMB contributed to the methodology; Dario K, Diego K, and PEV conceptualized the study; GML and MGB conceived the study and wrote the manuscript.

Acknowledgements
We would like to thank Rene Baron and Williams Foundation. We thank Adan Guerrero and Alberto Darszon for their insightful comments.

References

Alvau A, Battistone MA, Gervasi MG, Navarrete FA, Xu X, Sánchez-Cárdenas C, de la Vega-Beltran JL, da Ros VG, Greer PA, Darszon A, *et al.* 2016 The tyrosine kinase FER is responsible for the capacitation-associated increase in tyrosine phosphorylation in murine sperm. *Development* **143** 2325–2333. (https://doi.org/10.1242/dev.136499)

Austin CR 1951 Observations on the penetration of the sperm in the mammalian egg. *Australian Journal of Scientific Research. Ser. B* **4** 581–596. (https://doi.org/10.1071/bi9510581)

Bouwer MF, Hamilton KE, Jonker PB, Kuiper SR, Louters LL & Looyenga BD 2021 NMS-873 functions as a dual inhibitor of mitochondrial oxidative phosphorylation. *Biochimie* **185** 33–42. (https://doi.org/10.1016/j.biochi.2021.03.004)

Buffone MG, Foster JA & Gerton GL 2008 The role of the acrosomal matrix in fertilization. *International Journal of Developmental Biology* **52** 511–522. (https://doi.org/10.1387/ijdb.072532mb)

Buffone MG, Kim K-S, Doak BJ, Rodriguez-Miranda E & Gerton GL 2009 Functional consequences of cleavage, dissociation and exocytotic release of ZP3R, a C4BP-related protein, from the mouse sperm acrosomal matrix. *Journal of Cell Science* **122** 3153–3160. (https://doi.org/10.1242/jcs.052977)

Busso D, Cohen DJ, Maldera JA, Dematteis A & Cuasnicu PS 2007 A novel function for CRISP1 in rodent fertilization: involvement in sperm-zona pellucida interaction. *Biology of Reproduction* **77** 848–854. (https://doi.org/10.1095/biolreprod.107.061788)

Chang MC 1951 Fertilizing capacity of spermatozoa deposited into the fallopian tubes. *Nature* **168** 697–698. (https://doi.org/10.1038/168697b0)

Chou TF, Brown SJ, Minond D, Nordin BE, Li K, Jones AC, Chase P, Porubsky PR, Stoltz BM, Schoenen FJ, *et al.* 2011 Reversible inhibitor of p97, DBeQ, impairs both ubiquitin-dependent and autophagic protein clearance pathways. *PNAS* **108** 4834–4839. (https://doi.org/10.1073/pnas.1015312108)

Egerton M & Samelson LE 1994 Biochemical characterization of valosin-containing protein, a protein tyrosine kinase substrate in hematopoietic cells. *Journal of Biological Chemistry* **269** 11435–11441. (https://doi.org/10.1016/S0021-9258(19)78142-3)

Fang CJ, Gui L, Zhang X, Moen DR, Li K, Frankowski KJ, Lin HJ, Schoenen FJ & Chou TF 2015 Evaluating p97 inhibitor analogues for their domain-selectivity and potency against the p97-p47 complex. *ChemMedChem* **10** 52–56. (https://doi.org/10.1002/cmdc.201402420)

Ficarro S, Chertihin O, Westbrook VA, White F, Jayes F, Kalab P, Marto JA, Shabanowitz J, Herr JC, Hunt DF, *et al.* 2003 Phosphoproteome analysis of capacitated human sperm: evidence of tyrosine phosphorylation of a kinase-anchoring protein 3 and valosin-containing protein/p97 during capacitation. *Journal of Biological Chemistry* **278** 11579–11589. (https://doi.org/10.1074/jbc.M202325200)

Flesch FM, GB & Flesch F 2000 Dynamics of the mammalian sperm plasma membrane in the process of fertilization. *Biochimica et Biophysica Acta* **1469** 197–235. (https://doi.org/10.1016/s0304-4157(00)00018-6)

Gadella BMM 2008 Sperm membrane physiology and relevance for fertilization. *Animal Reproduction Science* **107** 229–236. (https://doi.org/10.1016/j.anireprosci.2008.05.006)

Gervasi MG & Visconti PE 2016 Chang's meaning of capacitation: a molecular perspective. *Molecular Reproduction and Development* **83** 860–874. (https://doi.org/10.1002/mrd.22663)

Geussova G, Kalab P & Peknicova J 2002 Valosine containing protein is a substrate of cAMP-activated boar sperm tyrosine kinase. *Molecular Reproduction and Development* **63** 366–375. (https://doi.org/10.1002/mrd.10156)

Halawani D, LeBlanc AC, Rouiller I, Michnick SW, Servant MJ & Latterich M 2009 Hereditary inclusion body myopathy-linked p97/VCP mutations in the NH2 domain and the D1 ring modulate p97/VCP ATPase activity and D2 ring conformation. *Molecular and Cellular Biology* **29** 4484–4494. (https://doi.org/10.1128/MCB.00252-09)

Hasuwa H, Muro Y, Ikawa M, Kato N, Tsujimoto Y & Okabe M 2010 Transgenic mouse sperm that have green acrosome and red mitochondria allow visualization of sperm and their acrosome reaction in vivo. *Experimental Animals* **59** 105–107. (https://doi.org/10.1538/expanim.59.105)

Herrero MB, Mandal A, Digilio LC, Coonrod SA, Maier B & Herr JC 2005 Mouse SLLP1, a sperm lysozyme-like protein involved in sperm-egg binding and fertilization. *Developmental Biology* **284** 126–142. (https://doi.org/10.1016/j.ydbio.2005.05.008)

Hirling H, Scheller RH, Barford D, Tonks NK, Fazel A, Posner BI, Paiement J & Bergeron JJM 1996 Phosphorylation of synaptic vesicle proteins: modulation of the alpha SNAP interaction with the core complex. *PNAS* **93** 11945–11949. (https://doi.org/10.1073/pnas.93.21.11945)

Hirohashi N, La Spina FAL, Romarowski A & Buffone MG 2015 Redistribution of the intra-acrosomal EGFP before acrosomal exocytosis in mouse spermatozoa. *Reproduction* **149** 657–663. (https://doi.org/10.1530/REP-15-0017)

Hunnicutt GR, Koppel DE & Myles DG 1997 Analysis of the process of localization of fertilin to the sperm posterior head plasma membrane domain during sperm maturation in the epididymis. *Developmental Biology* **191** 146–159. (https://doi.org/10.1006/dbio.1997.8700)

Jankovicova J, Frolikova M, Sebkova N, Simon M, Cupperova P, Lipcseyova D, Michalkova K, Horovska L, Sedlacek R, Stopka P, *et al.* 2016 Characterization of tetraspanin protein CD81 in mouse spermatozoa and bovine gametes. *Reproduction* **152** 785–793. (https://doi.org/10.1530/REP-16-0304)

Kondo H, Rabouille C, Newman R, Levine TP, Pappin D, Freemont P & Warren G 1997 p47 is a cofactor for p97-mediated membrane fusion. *Nature* **388** 75–78. (https://doi.org/10.1038/40411)

Leung MR, Ravi RT, Gadella BM & Zeev-Ben-Mordehai T 2021 Membrane remodeling and matrix dispersal intermediates during mammalian acrosomal exocytosis. *Frontiers in Cell and Developmental Biology* **9** 765673. (https://doi.org/10.3389/fcell.2021.765673).

Luque GM, Xu X, Romarowski A, Gervasi MG, Orta G, De la Vega-Beltrán JL, Stival C, Gilio N, Dalotto-Moreno T, Krapf D, *et al.* 2021 Cdc42 localized in the CatSper signaling complex regulates cAMP-dependent pathways in mouse sperm. *FASEB Journal* **35** e21723. (https://doi.org/10.1096/fj.202002773RR)

Luque GM, Schiavi-Ehrenhaus LJ, Jabloñski M, Balestrini PA, Novero AG, Torres NI, Osycka-Salut CE, Darszon A, Krapf D & Buffone MG 2023 High-throughput screening method for discovering CatSper inhibitors using membrane depolarization caused by external calcium chelation and fluorescent cell barcoding. *Frontiers in Cell and Developmental Biology* **11** 1010306. (https://doi.org/10.3389/fcell.2023.1010306).

Madeo F, Schlauer J, Zischka H, Mecke D & Fröhlich KU 1998 Tyrosine phosphorylation regulates cell cycle-dependent nuclear localization of Cdc48p. *Molecular Biology of the Cell* **9** 131–141. (https://doi.org/10.1091/mbc.9.1.131)

Mandal A, Klotz KL, Shetty J, Jayes FL, Wolkowicz MJ, Bolling LC, Coonrod SA, Black MB, Diekman AB, Haystead TAJ, *et al.* 2003 SLLP1, a unique, intra-acrosomal, non-bacteriolytic, c lysozyme-like protein of human spermatozoa. *Biology of Reproduction* **68** 1525–1537. (https://doi.org/10.1095/biolreprod.102.010108)

Matsuura M & Yogo K 2015 TMEM225: a possible protein phosphatase 1γ2 (PP1γ2) regulator localizes to the equatorial segment in mouse spermatozoa. *Molecular Reproduction and Development* **82** 139–148. (https://doi.org/10.1002/mrd.22453)

Miranda PV, Allaire A, Sosnik J & Visconti PE 2009 Localization of low-density detergent-resistant membrane proteins in intact and acrosome-reacted mouse sperm. *Biology of Reproduction* **80** 897–904. (https://doi.org/10.1095/biolreprod.108.075242)

Navarrete FA, García-Vázquez FA, Alvau A, Escoffier J, Krapf D, Sánchez-Cárdenas C, Salicioni AM, Darszon A & Visconti PE 2015 Biphasic role of calcium in mouse sperm capacitation signaling pathways. *Journal of Cellular Physiology* **230** 1758–1769. (https://doi.org/10.1002/jcp.24873)

Puga Molina LC, Pinto NA, Torres NI, Ana AL, Luque GM, Balestrini PA, Romarowski A, Krapf D, Santi CM, Treviño CL, *et al.* 2018 CFTR/ENaC-dependent regulation of membrane potential during human sperm capacitation is initiated by bicarbonate uptake through NBC. *Journal of Biological Chemistry* **293** 9924–9936. (https://doi.org/10.1074/jbc.RA118.003166)

Rabouille C, Levine TP, Peters JM & Warren G 1995 An NSF-like ATPase, p97, and NSF mediate cisternal regrowth from mitotic Golgi fragments. *Cell* **82** 905–914. (https://doi.org/10.1016/0092-8674(95)90270-8)

Romarowski A, Battistone MA, La Spina FA, Puga Molina Ldel C, Luque GM, Vitale AM, Cuasnicu PS, Visconti PE, Krapf D & Buffone MG 2015 PKA-dependent phosphorylation of LIMK1 and cofilin is essential for mouse sperm acrosomal exocytosis. *Developmental Biology* **405** 237–249. (https://doi.org/10.1016/j.ydbio.2015.07.008)

Satouh Y, Inoue N, Ikawa M & Okabe M 2012 Visualization of the moment of mouse sperm-egg fusion and dynamic localization of IZUMO1. *Journal of Cell Science* **125** 4985–4990. (https://doi.org/10.1242/jcs.100867)

Shih YT & Hsueh YP 2018 The involvement of endoplasmic reticulum formation and protein synthesis efficiency in VCP- and ATL1-related neurological disorders. *Journal of Biomedical Science* **25** 2. (https://doi.org/10.1186/s12929-017-0403-3).

Song WH, Yi YJ, Sutovsky M, Meyers S & Sutovsky P 2016 Autophagy and ubiquitin-proteasome system contribute to sperm mitophagy after mammalian fertilization. *PNAS* **113** E5261–E5270. (https://doi.org/10.1073/pnas.1605844113)

Sosnik J, Buffone MG & Visconti PE 2010 Analysis of CAPZA3 localization reveals temporally discrete events during the acrosome reaction. *Journal of Cellular Physiology* **224** 575–580. (https://doi.org/10.1002/jcp.22211)

Stival C, La Spina FA, Baró Graf C, Arcelay E, Arranz SE, Ferreira JJ, Le Grand S, Dzikunu VA, Santi CM, Visconti PE, *et al.* 2015 Src kinase is the connecting player between protein kinase A (PKA) activation and hyperpolarization through SLO3 potassium channel regulation in mouse sperm. *Journal of Biological Chemistry* **290** 18855–18864. (https://doi.org/10.1074/jbc.M115.640326)

Stival C, Puga Molina Ldel C, Paudel B, Buffone MG, Visconti PE & Krapf D 2016 Sperm capacitation and acrosome reaction in mammalian sperm. *Advances in Anatomy, Embryology, and Cell Biology* **220** 93–106.

Toshimori K, Tanii I, Araki S & Oura C 1992 Characterization of the antigen recognized by a monoclonal antibody MN9: unique transport pathway to the equatorial segment of sperm head during spermiogenesis. *Cell and Tissue Research* **270** 459–468. (https://doi.org/10.1007/BF00645047)

Urbé S, Page LJ & Tooze SA 1998 Homotypic fusion of immature secretory granules during maturation in a cell-free assay. *Journal of Cell Biology* **143** 1831–1844. (https://doi.org/10.1083/jcb.143.7.1831)

Visconti PE, Moore GD, Bailey JL, Leclerc P, Connors SA, Pan D, Olds-Clarke P & Kopf GS 1995 Capacitation of mouse spermatozoa. II. Protein tyrosine phosphorylation and capacitation are regulated by a cAMP-dependent pathway. *Development* **121** 1139–1150. (https://doi.org/10.1242/dev.121.4.1139)

White SR & Lauring B 2007 AAA+ ATPases: achieving diversity of function with conserved machinery. *Traffic* **8** 1657–1667. (https://doi.org/10.1111/j.1600-0854.2007.00642.x)

Zhang X, Shaw A, Bates PA, Newman RH, Gowen B, Orlova E, Gorman MA, Kondo H, Dokurno P, Lally J, *et al.* 2000 Structure of the AAA ATPase p97. *Molecular Cell* **6** 1473–1484. (https://doi.org/10.1016/s1097-2765(00)00143-x)